The Little–Hopfield model on a sparse random graph

2004 J. Phys. A: Math. Gen. 37 9087

(http://iopscience.iop.org/0305-4470/37/39/003)

INSTITUTE OF PHYSICS PUBLISHING JOURNAL OF PHYSICS A: MATHEMATICAL AND GENERAL

J. Phys. A: Math. Gen. **37** (2004) 9087–9099 PII: S0305-4470(04)69585-0

The Little–Hopfield model on a sparse random graph

I Pérez Castillo and N S Skantzos

Institute for Theoretical Physics, Celestijnenlaan 200D, Katholieke Universiteit Leuven, Leuven B-3001, Belgium

Received 29 September 2003, in final form 23 July 2004
Published 15 September 2004
Online at stacks.iop.org/JPhysA/37/9087
doi:10.1088/0305-4470/37/39/003

Abstract

We study the Hopfield model on a random graph in scaling regimes where the average number of connections per neuron is a finite number and the spin dynamics is governed by a synchronous execution of the microscopic update rule (Little–Hopfield model). We solve this model within replica symmetry, and by using bifurcation analysis we prove that the spin-glass/paramagnetic and the retrieval/paramagnetic transition lines of our phase diagram are identical to those of sequential dynamics. The first-order retrieval/spin-glass transition line follows by direct evaluation of our observables using population dynamics. Within the accuracy of numerical precision and for sufficiently small values of the connectivity parameter we find that this line coincides with the corresponding sequential one. Comparison with simulation experiments shows excellent agreement.

PACS numbers: 87.18.Sn, 02.10.Ox, 05.50.+q, 75.10.Nr

1. Introduction

Since the first analytical work describing pattern recall was presented and the theoretical foundations describing the operation of neural networks were subsequently set, the progress in the field of attractor neural network models has been advancing, revealing interesting properties. Early analytical attempts to solve non-trivial neural network systems were analytically constrained to the study of fully-connected ones. From a real (i.e. biological) point of view one would ideally prefer to study models of sparse connectivity. Subsequently, theoretical work turned (among other directions) to sparse models and, in particular, to the so-called extremely diluted ones [1]. These could still be solved exactly owing to the simplification of considering system sizes exponentially bigger than the average connectivity per neuron (while both of these numbers were eventually sent to infinity).

One direction in developing the neural network theory further towards realism implies moving away from the simplifications made in extremely diluted systems and considering *finite* degrees of connectivity. This, however, appears to be a highly non-trivial step ahead

since at an early stage of solving the relevant equations one is confronted with more than the two traditional observables (the magnetization and the overlap); in fact, one is required to consider an order-parameter function.

Although initial attempts to solve such models showed the underlying analytical complexity [2, 3], the more refined mathematical tools were only relatively recently developed and in fact for applications different from neural networks (for instance, for optimization problems [4] or error-correcting codes [5]). The first study which applied the finite-connectivity methodology to neural network problems has been very recently presented in [6], where phase diagrams were presented for a variety of synaptic kernels. There, the authors study neural networks in which the microscopic neuronal dynamics is a sequential execution of an update rule (describing alignment to post-synaptic potentials). In this paper we examine the effect of choosing a *synchronous* microscopic dynamics in Hopfield models of finite connectivity, i.e. one in which neurons are updated in parallel at each time step. The equilibrium properties of the parallel and sequential dynamics Hopfield model were first studied in the parameter regime of the so-called extreme dilution [10, 11]. These two different types of dynamics are known to share very interesting properties. For instance, in simple ferromagnetic models one can prove that thermodynamic observables become identical [7]. It is yet unclear to what extent the two types of dynamical models share these common equilibrium features. For example, it is known that the phase diagram of the synchronous Hopfield model changes [8, 9][1] whereas that of the Sherrington–Kirkpatrick model remains unaffected [12].

This paper is organized as follows: in the following section we present definitions of our model. In section 3 we derive the saddle point equations for the free energy and make our replica-symmetric ansatz. In section 4 we give expressions of the free energy in terms of the replica symmetric order function whereas our results and phase diagrams are given in section 5.

2. Definitions

We study neural network models of N binary neurons $\boldsymbol{\sigma} = (\sigma_1, \ldots, \sigma_N)$ with $\sigma_i = -1$ representing 'at rest' and $\sigma_i = 1$ the 'firing' state. The miscroscopic neuron dynamics is a stochastic alignment to 'local fields' (the post-synaptic potentials) in which updates in neuronal states are made for all $i \in \{1, \ldots, N\}$ in a fully synchronous way at each discrete time step:

$$\text{Prob}[\sigma_i(t+1) = \pm 1] = \tfrac{1}{2}[1 \pm \tanh(\beta h_i(\boldsymbol{\sigma}(t)))] \tag{1}$$

where $h_i(\boldsymbol{\sigma}(t)) = \sum_j J_{ij}\sigma_j(t)$. The parameter $\beta \in [0, \infty)$ controls the amount of thermal noise in the dynamics with $\beta = \infty$ corresponding to a fully deterministic execution of (1) and $\beta = 0$ to a fully random execution. The quantities J_{ij} describe interaction couplings. If one expresses (1) in terms of the microscopic state probabilities $p_t(\boldsymbol{\sigma})$:

$$p_{t+1}(\boldsymbol{\sigma}) = \sum_{\boldsymbol{\sigma}'} W[\boldsymbol{\sigma}; \boldsymbol{\sigma}'] p_t(\boldsymbol{\sigma}') \qquad W[\boldsymbol{\sigma}; \boldsymbol{\sigma}'] = \prod_{i=1}^{N} \frac{\mathrm{e}^{\beta\sigma_i h_i(\boldsymbol{\sigma}')}}{2\cosh[\beta h_i(\boldsymbol{\sigma}')]} \tag{2}$$

then, for any finite β and finite N the process (2) is ergodic and evolves to a unique distribution $p_\infty(\boldsymbol{\sigma})$. It can be shown that this is a unique equilibrium state (obeying detailed balance)

[1] This difference seems to be an artefact of the replica symmetric approximation. The two phase diagrams become identical within full replica symmetry breaking [8], although it is unclear at which stage of the breaking scheme this occurs.

if and only if $J_{ij} = J_{ji}$ [16].[2] At equilibrium, the microscopic state probabilities acquire the form $p_\infty \sim \exp[-\beta H(\boldsymbol{\sigma})]$, where

$$H(\boldsymbol{\sigma}) = -\frac{1}{\beta}\sum_i \log[2\cosh(\beta h_i(\boldsymbol{\sigma}))] \tag{3}$$

is the Hamiltonian. For the interactions J_{ij} we now take

$$J_{ij} = \frac{c_{ij}}{c}\sum_{\mu=1}^{p}\xi_i^\mu \xi_j^\mu. \tag{4}$$

This corresponds to storing p memories $\boldsymbol{\xi}_i = \left(\xi_i^1, \ldots, \xi_i^p\right) \in \{-1, 1\}^p$ among the synapses in a Hebbian-type way. The variables $c_{ij} \in \{0, 1\}$ with $c_{ij} = c_{ji}$ represent dilution, while $c = (1/N)\sum_{i,j} c_{ij}$ corresponds to the average connectivity of the network. Models of the type (4) with $c \to \infty$ (while $c \sim \log N$) are known as extremely diluted and due to their simplicity have been studied extensively (see for instance [10, 11, 13–15] and references therein). What is less known are properties of these systems in the non-trivial scaling regime of *finite connectivity* where $c \sim \mathcal{O}(1)$ (with the probability $c/N \to 0$). Due to the complicated methodology required such systems have only recently been studied in [6] where a thorough bifurcation analysis was performed and phase diagrams were derived. For the distribution of the random variable c_{ij} we will consider

$$P(c_{ij}) = \frac{c}{N}\delta_{c_{ij},1} + \left(1 - \frac{c}{N}\right)\delta_{c_{ij},0} \tag{5}$$

for all pairs (i, j). All thermodynamic quantities will have to be averaged over (5). Note that due to the system's sparse connectivity the number of patterns can only be finite.

To derive observable quantities we will calculate the free energy per neuron $f = -\lim_{N\to\infty}\frac{1}{\beta N}\langle\log\sum_{\boldsymbol{\sigma}} \mathrm{e}^{-\beta H(\boldsymbol{\sigma})}\rangle_{\{c_{ij}\}}$, with $\langle\cdots\rangle$ denoting the average over the distribution of dilution variables. As in all synchronous dynamics models, the evaluation of the free energy is greatly simplified by introducing an extra set of spins so that f can be rewritten as

$$f = -\lim_{N\to\infty}\frac{1}{\beta N}\left\langle\log\sum_{\boldsymbol{\sigma}\boldsymbol{\tau}}\mathrm{e}^{-\beta\mathcal{H}(\boldsymbol{\sigma},\boldsymbol{\tau})}\right\rangle_{\{c_{ij}\}} \qquad \mathcal{H}(\boldsymbol{\sigma},\boldsymbol{\tau}) = -\sum_{ij}\sigma_i J_{ij}\tau_j. \tag{6}$$

Equation (6) will be the starting point for our analysis.

3. Saddle-point equations

In order to calculate the free energy (6) we begin by invoking the replica identity $\langle\log Z\rangle = \lim_{n\to 0}\frac{1}{n}\log\langle Z^n\rangle$. One can then take the average over the dilution variables resulting in

$$f = -\lim_{N\to\infty}\lim_{n\to 0}\frac{1}{\beta N n}\log\sum_{\boldsymbol{\sigma}^1\cdots\boldsymbol{\sigma}^n}\sum_{\boldsymbol{\tau}^1\cdots\boldsymbol{\tau}^n} \times\exp\left[\frac{c}{2N}\sum_{ij}\left(\exp\left(\frac{\beta}{c}(\boldsymbol{\xi}_i\cdot\boldsymbol{\xi}_j)\sum_\alpha\left(\sigma_i^\alpha\tau_j^\alpha + \sigma_j^\alpha\tau_i^\alpha\right)\right) - 1\right)\right] \tag{7}$$

where $\boldsymbol{\xi}_i\cdot\boldsymbol{\xi}_j = \sum_\mu \xi_i^\mu\xi_j^\mu$. Note that at this stage an exponential has appeared as an argument of another exponential. Here, effectively, the innermost exponential introduces an infinite

[2] Note that, unlike sequential models where detailed balance requires the exclusion of self-interactions, this is not a prerequisite here. However, due to the scaling regime of finite connectivity terms originating from the self-interacting part will for $N \to \infty$ give a vanishing contribution to thermodynamic quantities.

number of observables. However, unlike systems of full connectivity or of extreme dilution where only the linear and quadratic observables (order parameters) *survive* in the limit $N \to \infty$, all cumulants play a role here. They can be recast in an order-parameter function. This complication is a direct consequence of the scaling regime of finite connectivity.

It is now convenient to use the concept of sublattices [17] which divide the space of sites into 2^p groups $I_{\boldsymbol{\xi}} = \{i | \boldsymbol{\xi}_i = \boldsymbol{\xi}\}$. We define $\boldsymbol{\sigma}_i = \left(\sigma_i^1, \ldots, \sigma_i^n\right)$ and abbreviate the averages over the sublattices by $\langle F(\boldsymbol{\xi})\rangle_{\boldsymbol{\xi}} = \sum_{\boldsymbol{\xi}} p_{\boldsymbol{\xi}} F(\boldsymbol{\xi})$ with the probabilities $p_{\boldsymbol{\xi}} \equiv |I_{\boldsymbol{\xi}}|/N$. Then the free energy becomes

$$f = -\lim_{N\to\infty}\lim_{n\to 0}\frac{1}{\beta N n}\log \sum_{\boldsymbol{\sigma}^1\cdots\boldsymbol{\sigma}^n}\sum_{\boldsymbol{\tau}^1\cdots\boldsymbol{\tau}^n} \times \exp\left[\frac{c}{2N}\sum_{\boldsymbol{\sigma}\boldsymbol{\sigma}'}\sum_{\boldsymbol{\tau}\boldsymbol{\tau}'}\sum_{\boldsymbol{\xi}\boldsymbol{\xi}'}\left(\exp\left(\frac{\beta}{c}(\boldsymbol{\xi}\cdot\boldsymbol{\xi}')\sum_{\alpha}(\sigma_\alpha\tau'_\alpha+\sigma'_\alpha\tau_\alpha)\right)-1\right) \times \sum_{i\in I_{\boldsymbol{\xi}}}\delta_{\boldsymbol{\sigma},\boldsymbol{\sigma}_i}\delta_{\boldsymbol{\tau},\boldsymbol{\tau}_i}\sum_{j\in I_{\boldsymbol{\xi}'}}\delta_{\boldsymbol{\sigma}',\boldsymbol{\sigma}_j}\delta_{\boldsymbol{\tau}',\boldsymbol{\tau}_j}\right]. \tag{8}$$

We now see that an order function has emerged which we introduce into our expression via

$$1 = \int\prod_{\boldsymbol{\xi}\boldsymbol{\sigma}\boldsymbol{\tau}}\left\{dP_{\boldsymbol{\xi}}(\boldsymbol{\sigma},\boldsymbol{\tau})\delta\left[P_{\boldsymbol{\xi}}(\boldsymbol{\sigma},\boldsymbol{\tau})-\frac{1}{|I_{\boldsymbol{\xi}}|}\sum_{i\in I_{\boldsymbol{\xi}}}\delta_{\boldsymbol{\sigma},\boldsymbol{\sigma}_i}\delta_{\boldsymbol{\tau},\boldsymbol{\tau}_i}\right]\right\}. \tag{9}$$

In the above expression we replace the δ-function by its integral representation (which introduces the conjugate order-parameter function $\hat{P}_{\boldsymbol{\xi}}(\boldsymbol{\sigma},\boldsymbol{\tau})$). We then perform the trace over the spin variables and take the limit $N \to \infty$ in our equations, resulting in the extremization problem:

$$f = -\lim_{n\to 0}\frac{1}{\beta n}\mathrm{Extr}_{\{P,\hat{P}\}}\left\{\left\langle\sum_{\boldsymbol{\sigma}\boldsymbol{\tau}}P_{\boldsymbol{\xi}}(\boldsymbol{\sigma},\boldsymbol{\tau})\hat{P}_{\boldsymbol{\xi}}(\boldsymbol{\sigma},\boldsymbol{\tau})\right\rangle_{\boldsymbol{\xi}}+\left\langle\log\left[\sum_{\boldsymbol{\sigma}\boldsymbol{\tau}}\mathrm{e}^{-\hat{P}_{\boldsymbol{\xi}}(\boldsymbol{\sigma},\boldsymbol{\tau})}\right]\right\rangle_{\boldsymbol{\xi}}\right. \tag{10}$$

$$\left.+\frac{c}{2}\left\langle\sum_{\boldsymbol{\sigma}\boldsymbol{\tau}}\sum_{\boldsymbol{\sigma}'\boldsymbol{\tau}'}P_{\boldsymbol{\xi}}(\boldsymbol{\sigma},\boldsymbol{\tau})P_{\boldsymbol{\xi}'}(\boldsymbol{\sigma}',\boldsymbol{\tau}')\left[\exp\left(\frac{\beta}{c}(\boldsymbol{\xi}\cdot\boldsymbol{\xi}')\sum_{\alpha}(\sigma_\alpha\tau'_\alpha+\sigma'_\alpha\tau_\alpha)\right)-1\right]\right\rangle_{\boldsymbol{\xi}\boldsymbol{\xi}'}\right\}. \tag{11}$$

Variation with respect to the densities $P_{\boldsymbol{\xi}}(\boldsymbol{\sigma},\boldsymbol{\tau})$ and $\hat{P}_{\boldsymbol{\xi}}(\boldsymbol{\sigma},\boldsymbol{\tau})$ gives the self-consistent equation

$$P_{\boldsymbol{\xi}}(\boldsymbol{\sigma},\boldsymbol{\tau}) = \frac{\exp\left[c\left\langle\sum_{\boldsymbol{\sigma}'\boldsymbol{\tau}'}P_{\boldsymbol{\xi}'}(\boldsymbol{\sigma}',\boldsymbol{\tau}')\left(\exp\left(\frac{\beta}{c}(\boldsymbol{\xi}\cdot\boldsymbol{\xi}')\sum_{\alpha}(\sigma_\alpha\tau'_\alpha+\sigma'_\alpha\tau_\alpha)\right)-1\right)\right\rangle_{\boldsymbol{\xi}'}\right]}{\sum_{\boldsymbol{\sigma}'\boldsymbol{\tau}'}\exp\left[c\left\langle\sum_{\boldsymbol{\sigma}''\boldsymbol{\tau}''}P_{\boldsymbol{\xi}''}(\boldsymbol{\sigma}'',\boldsymbol{\tau}'')\left(\exp\left(\frac{\beta}{c}(\boldsymbol{\xi}\cdot\boldsymbol{\xi}'')\sum_{\alpha}(\sigma'_\alpha\tau''_\alpha+\sigma''_\alpha\tau'_\alpha)\right)-1\right)\right\rangle_{\boldsymbol{\xi}''}\right]} \tag{12}$$

and also allows us to eliminate $\hat{P}_{\boldsymbol{\xi}}(\boldsymbol{\sigma},\boldsymbol{\tau})$ from the expression of the free energy which now becomes

$$f = \lim_{n\to 0}\frac{1}{\beta n}\mathrm{Extr}\left\{\frac{c}{2}\left\langle\sum_{\boldsymbol{\sigma}\boldsymbol{\tau}}\sum_{\boldsymbol{\sigma}'\boldsymbol{\tau}'}P_{\boldsymbol{\xi}}(\boldsymbol{\sigma},\boldsymbol{\tau})P_{\boldsymbol{\xi}'}(\boldsymbol{\sigma}',\boldsymbol{\tau}')\right.\right. \times\left(\exp\left(\frac{\beta}{c}(\boldsymbol{\xi}\cdot\boldsymbol{\xi}')\sum_{\alpha}(\sigma_\alpha\tau'_\alpha+\sigma'_\alpha\tau_\alpha)\right)-1\right)\Bigg\rangle_{\boldsymbol{\xi}\boldsymbol{\xi}'}-\left\langle\log\sum_{\boldsymbol{\sigma}\boldsymbol{\tau}}\exp\left[c\left\langle\sum_{\boldsymbol{\sigma}'\boldsymbol{\tau}'}P_{\boldsymbol{\xi}'}(\boldsymbol{\sigma}',\boldsymbol{\tau}')\right.\right.\right. \times\left.\left.\left.\left(\exp\left(\frac{\beta}{c}(\boldsymbol{\xi}\cdot\boldsymbol{\xi}')\sum_{\alpha}(\sigma_\alpha\tau'_\alpha+\sigma'_\alpha\tau_\alpha)\right)-1\right)\Bigg\rangle_{\boldsymbol{\xi}'}\right]\Bigg\rangle_{\boldsymbol{\xi}}\right\}. \tag{13}$$

This expression requires knowledge of the densities $P_\xi(\boldsymbol{\sigma}, \boldsymbol{\tau})$. However, the evaluation of the self-consistent equation (12) is an impossible task unless a further simplification is made. To proceed further we will make an assumption about the form of the densities $P_\xi(\boldsymbol{\sigma}, \boldsymbol{\tau})$. In the spirit of replica symmetry (RS) we will consider that permutation of spins within different replicas leave the order parameters invariant. Here, however, due to the presence of two species of spins we will also require that within the same replica group permutation of the states of σ_α and τ_α also leave for all α $P_\xi(\boldsymbol{\sigma}, \boldsymbol{\tau})$ invariant:

$$P_\xi(\boldsymbol{\sigma}, \boldsymbol{\tau}) = \int \frac{\mathrm{d}h\,\mathrm{d}r\,\mathrm{d}t}{[\mathcal{N}(h, r, t)]^n} W_\xi(h, r, t) \exp\left(\beta h \sum_\alpha \sigma_\alpha + \beta r \sum_\alpha \tau_\alpha + \beta t \sum_\alpha \sigma_\alpha \tau_\alpha\right) \tag{14}$$

where $\mathcal{N}(h, r, t)$ is the corresponding normalization constant

$$\mathcal{N}(h, r, t) = 4\cosh(\beta h)\cosh(\beta r)\cosh(\beta t) + 4\sinh(\beta h)\sinh(\beta r)\sinh(\beta t). \tag{15}$$

Let us finally turn to our system's macroscopic observables. Our replicated sublattice overlaps will be given by

$$m_\lambda^{\mu\alpha} = \left\langle \xi^\mu m_\xi^{\lambda,\alpha} \right\rangle_\xi \tag{16}$$

with the sublattice magnetizations defined as

$$m_\xi^{\lambda,\alpha} = \sum_{\sigma\tau} P_\xi(\boldsymbol{\sigma}, \boldsymbol{\tau}) \lambda^\alpha \tag{17}$$

with $\lambda = \sigma, \tau$. In RS the above quantities are the same for all values of the replica index. Thereafter we will drop the index α for notational simplicity. The observables (16) will be generated from the densities $P_\xi(\boldsymbol{\sigma}, \boldsymbol{\tau})$. In general, from $P_\xi(\boldsymbol{\sigma}, \boldsymbol{\tau})$ one can evaluate all higher-order observables

$$L_\xi^{\alpha_1 \cdots \alpha_m; \gamma_1 \cdots \gamma_\ell} = \sum_{\sigma\tau} P_\xi(\boldsymbol{\sigma}, \boldsymbol{\tau}) \sigma^{\alpha_1} \cdots \sigma^{\alpha_m} \tau^{\gamma_1} \cdots \tau^{\gamma_\ell}. \tag{18}$$

Working out the simplest of these using the RS ansatz (14) gives

$$\begin{aligned} m_\sigma^\mu &\equiv \left\langle \xi^\mu \sum_{\sigma\tau} P_\xi(\boldsymbol{\sigma}, \boldsymbol{\tau}) \sigma^{\alpha_1} \right\rangle_\xi \\ &= \left\langle \xi^\mu \int \mathrm{d}h\,\mathrm{d}r\,\mathrm{d}t\, W_\xi(h, r, t) \frac{\tanh(\beta h) + \tanh(\beta r)\tanh(\beta t)}{1 + \tanh(\beta t)\tanh(\beta r)\tanh(\beta h)} \right\rangle_\xi \end{aligned} \tag{19}$$

$$\begin{aligned} q_{\sigma\sigma} &\equiv \left\langle \sum_{\sigma\tau} P_\xi(\boldsymbol{\sigma}, \boldsymbol{\tau}) \sigma^{\alpha_1} \sigma^{\alpha_2} \right\rangle_\xi \\ &= \left\langle \int \mathrm{d}h\,\mathrm{d}r\,\mathrm{d}t\, W_\xi(h, r, t) \left[\frac{\tanh(\beta h) + \tanh(\beta r)\tanh(\beta t)}{1 + \tanh(\beta t)\tanh(\beta r)\tanh(\beta h)} \right]^2 \right\rangle_\xi \end{aligned} \tag{20}$$

and similar expressions follow for the observables m_τ^μ, $q_{\tau\tau}$ and $q_{\sigma\tau}$.

4. The self-consistent equation and the free energy

4.1. Derivation of the self-consistent equation

In order to arrive at a self-consistent equation for the densities $W_\xi(h, r, t)$ we first substitute the RS ansatz (14) into (12). Then, following [6], we isolate the occurrences of quantities of

the form $\sum_\alpha \sigma_\alpha$, $\sum_\alpha \tau_\alpha$ and $\sum_\alpha \sigma_\alpha \tau_\alpha$ by inserting

$$1 = \sum_{m_\sigma=-\infty}^{\infty} \int_0^{2\pi} \frac{\mathrm{d}\hat{m}_\sigma}{2\pi} \exp\left(\mathrm{i}\hat{m}_\sigma \left(m_\sigma - \sum_\alpha \sigma_\alpha\right)\right) \tag{21}$$

$$1 = \sum_{m_\tau=-\infty}^{\infty} \int_0^{2\pi} \frac{\mathrm{d}\hat{m}_\tau}{2\pi} \exp\left(\mathrm{i}\hat{m}_\tau \left(m_\tau - \sum_\alpha \tau_\alpha\right)\right) \tag{22}$$

$$1 = \sum_{q=-\infty}^{\infty} \int_0^{2\pi} \frac{\mathrm{d}\hat{q}}{2\pi} \exp\left(\mathrm{i}\hat{q} \left(q - \sum_\alpha \sigma_\alpha \tau_\alpha\right)\right). \tag{23}$$

After some algebra we can take the limit $n \to 0$ in our equations and arrive at

$$\begin{aligned}\int \mathrm{d}W_{\boldsymbol{\xi}}(h,r,t) \exp(\beta h m_\sigma + \beta r m_\tau + \beta t q) \\ = \exp\left[c\left\langle \int \mathrm{d}W_{\boldsymbol{\xi}'}(h',r',t')(\exp(m_\sigma K_1(h',r',t';\boldsymbol{\xi}\cdot\boldsymbol{\xi}') \right.\right. \\ \left.\left. + m_\tau K_2(h',r',t';\boldsymbol{\xi}\cdot\boldsymbol{\xi}') + q K_3(h',r',t';\boldsymbol{\xi}\cdot\boldsymbol{\xi}')) - 1)\right\rangle_{\boldsymbol{\xi}'}\right]\end{aligned} \tag{24}$$

where we have used the notation $\mathrm{d}W_{\boldsymbol{\xi}}(h,r,t) = \mathrm{d}h\,\mathrm{d}r\,\mathrm{d}t\,W_{\boldsymbol{\xi}}(h,r,t)$ and introduced

$$K_1(h',r',t';\boldsymbol{\xi}\cdot\boldsymbol{\xi}') = \frac{1}{4}\log\frac{\Omega_{++}\Omega_{+-}}{\Omega_{-+}\Omega_{--}} \tag{25}$$

$$K_2(h',r',t';\boldsymbol{\xi}\cdot\boldsymbol{\xi}') = \frac{1}{4}\log\frac{\Omega_{++}\Omega_{-+}}{\Omega_{+-}\Omega_{--}} \tag{26}$$

$$K_3(h',r',t';\boldsymbol{\xi}\cdot\boldsymbol{\xi}') = \frac{1}{4}\log\frac{\Omega_{++}\Omega_{--}}{\Omega_{+-}\Omega_{-+}} \tag{27}$$

with

$$\begin{aligned}\Omega_{\sigma\tau} \equiv \Omega_{\sigma\tau}(h',r',t';\boldsymbol{\xi}\cdot\boldsymbol{\xi}') = 4\cosh\left[\beta h' + \sigma\frac{\beta}{c}(\boldsymbol{\xi}\cdot\boldsymbol{\xi}')\right]\cosh\left[\beta r' + \tau\frac{\beta}{c}(\boldsymbol{\xi}\cdot\boldsymbol{\xi}')\right]\cosh[\beta t'] \\ + 4\sinh\left[\beta h' + \sigma\frac{\beta}{c}(\boldsymbol{\xi}\cdot\boldsymbol{\xi}')\right]\sinh\left[\beta r' + \tau\frac{\beta}{c}(\boldsymbol{\xi}\cdot\boldsymbol{\xi}')\right]\sinh[\beta t'].\end{aligned} \tag{28}$$

Performing an inverse Fourier transform to (24), expanding the right-hand side and integrating over the magnetizations m_σ, m_τ and the overlap q, we obtain

$$\begin{aligned}W_{\boldsymbol{\xi}}(h,r,t) = \sum_{k=0}^{\infty}\frac{\mathrm{e}^{-c}c^k}{k!}\left\langle\cdots\left\langle\int\left[\prod_{l=1}^{k}\mathrm{d}W_{\boldsymbol{\xi}^l}(h'_l,r'_l,t'_l)\right]\right.\right. \\ \times\delta\left[h - \frac{1}{\beta}\sum_{l=1}^{k}K_1(h'_l,r'_l,t'_l;\boldsymbol{\xi}\cdot\boldsymbol{\xi}^l)\right]\delta\left[r - \frac{1}{\beta}\sum_{l=1}^{k}K_2(h'_l,r'_l,t'_l;\boldsymbol{\xi}\cdot\boldsymbol{\xi}^l)\right] \\ \left.\left.\times\delta\left[t - \frac{1}{\beta}\sum_{l=1}^{k}K_3(h'_l,r'_l,t'_l;\boldsymbol{\xi}\cdot\boldsymbol{\xi}^l)\right]\right\rangle_{\boldsymbol{\xi}^1}\cdots\right\rangle_{\boldsymbol{\xi}^k}.\end{aligned} \tag{29}$$

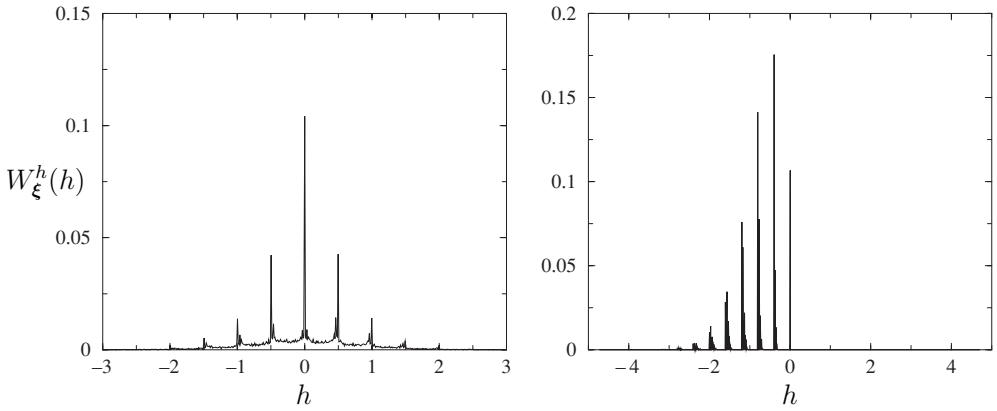

Figure 1. Typical profiles of the marginal densities $W^h_\xi(h)$ for $p = 6$, $c = 4$, $T = 0.1$ (left picture, corresponding to the spin-glass region of figure 2) and for $p = 2$, $c = 5$, $T = 0.1$ (right picture, corresponding to the retrieval region of figure 2). Note that since p is even the peaks are located at $h = 2l/c$ with l integer.

Expression (29) is the final result from which we evaluate the densities $W_\xi(h, r, t)$. Although appearing to be a daunting numerical task it can be evaluated using the simple algorithm of 'population dynamics' as described e.g. in [18]. This relies on the local 'tree-like' structure of finitely-connected networks of spins and it consists of having a large population of triplets (h_l, r_l, t_l) which are to be updated for a large number of iteration steps in the following way: one first selects a number k from a Poisson distribution of mean c. Then, one chooses $l = 1, \ldots, k$ triplets (h_l, r_l, t_l) and l sublattices $\boldsymbol{\xi}^l$ at random and calculates the expressions appearing in the delta functions. Finally, one selects a new triplet (h, r, t) and a new sublattice $\boldsymbol{\xi}$ at random, and updates them using the calculated expressions.

To get an idea about the profile of the densities $W_\xi(h, r, t)$ we have applied the previous algorithm to study the marginal densities $W^h_\xi(h) = \int \mathrm{d}r\, \mathrm{d}t\, W_\xi(h, r, t)$, $W^r_\xi(r) = \int \mathrm{d}h\, \mathrm{d}t\, W_\xi(h, r, t)$ and $W^t_\xi(t) = \int \mathrm{d}h\, \mathrm{d}r\, W_\xi(h, r, t)$. First, we observe that close to the zero-temperature limit the marginals $W^h_\xi(h)$ and $W^r_\xi(r)$ become a collection of delta peaks; in this limit, due to the absence of thermal noise, the effective fields $\{h, r\}$ become identical to the *true* local fields. Since the average number of connections per neuron is here a finite number and the couplings are discrete, the local fields are a multiple integer[3] [3] of $1/c$ (see figure 1 for typical profiles of the marginal densities). As one moves away from the $T = 0$ regime the profile of the marginal densities $W^h_\xi(h)$ and $W^r_\xi(r)$ takes a non-trivial form until the paramagnetic phase is reached where one observes that $W^h_\xi(x) = W^r_\xi(x) = W^t_\xi(x) = \delta(x)$, as it should. We have numerically evaluated the above marginals for several regions of the parameter space and it is interesting to note that $W^h_\xi(h)$ and $W^r_\xi(r)$ are identical (within the accuracy of numerical precision)[4] whereas $W^t_\xi(t) = \delta(t)$. The latter implies that our RS ansatz can be simplified further. However, this result relies on numerical observations and a rigorous analytical proof appears somewhat hard (one cannot rely on an induction proof since at the first iteration step of (29) the fields t must take a non-zero value). Nevertheless, it is interesting to note that setting $t = 0$ to (29) completely decouples the density $W_\xi(h, r, t)$ to two identical

[3] In fact, for even number of patterns p we have that the local fields present peaks at $2l/c$ with l integer, while for odd p we have l/c.

[4] This is of course expected since the Hamiltonian (6) is invariant under the interchange of the two spin species.

densities

$$Q_{\boldsymbol{\xi}}(x) = \sum_{k=0}^{\infty} \frac{\mathrm{e}^{-c} c^k}{k!} \left\langle \left\langle \cdots \int \left[\prod_{l=1}^{k} \mathrm{d}x_l \, Q_{\boldsymbol{\xi}^l}(x_l) \right] \right.\right.$$
$$\left.\left. \times \delta \left[x - \frac{1}{\beta} \sum_{l=1}^{k} \mathrm{ath} \left(\tanh[\beta x_l] \tanh \left[\frac{\beta}{c} (\boldsymbol{\xi} \cdot \boldsymbol{\xi}^l) \right] \right) \right] \right\rangle_{\boldsymbol{\xi}^1} \cdots \right\rangle_{\boldsymbol{\xi}^k} \tag{30}$$

with $x = \{h, r\}$. Note that this equation is now the same as the one that follows from the analysis of [6], as it should.

4.2. The free energy

Let us now express the free energy (13) as function of the densities $W_{\boldsymbol{\xi}}(h, r, t)$. The first term comprising (13) (energetic part) can be calculated without difficulty. One uses the RS ansatz (14) to replace the distributions $P_{\boldsymbol{\xi}}(\boldsymbol{\sigma}, \boldsymbol{\tau})$ by the densities $W_{\boldsymbol{\xi}}(h, r, t)$ and subsequently one performs the spins summations and takes the limit $n \to 0$. The second term is slightly more complicated. First, we expand the exponential function. This replicates the traces over the spins and sublattice variables. Inserting then for each of the replicated densities the RS ansatz (14) leads to

$$\left\langle \log \sum_{\boldsymbol{\sigma}\boldsymbol{\tau}} \exp \left[c \left\langle \sum_{\hat{\boldsymbol{\sigma}}\hat{\boldsymbol{\tau}}} P_{\boldsymbol{\xi}'}(\hat{\boldsymbol{\sigma}}, \hat{\boldsymbol{\tau}}) \left(\exp \left(\frac{\beta J}{c} (\boldsymbol{\xi} \cdot \boldsymbol{\xi}') \sum_{\alpha} (\sigma_\alpha \hat{\tau}_\alpha + \hat{\sigma}_\alpha \tau_\alpha) \right) - 1 \right) \right\rangle_{\boldsymbol{\xi}'} \right] \right\rangle_{\boldsymbol{\xi}}$$
$$= \left\langle \log \sum_{k=0}^{\infty} \frac{\mathrm{e}^{-c} c^k}{k!} \left\langle \cdots \left\langle \int \left[\prod_{l=1}^{k} \mathrm{d}W_{\boldsymbol{\xi}^l}(h_l, r_l, t_l) \right] \prod_{\alpha=1}^{n} \sum_{\sigma_\alpha \tau_\alpha} \prod_{l=1}^{k} \sum_{\hat{\sigma}_\alpha^l \hat{\tau}_\alpha^l} \right.\right.\right.$$
$$\left.\left.\left. \times \exp \left(\frac{\beta}{c} (\boldsymbol{\xi} \cdot \boldsymbol{\xi}^l) \left(\sigma_\alpha \hat{\tau}_\alpha^l + \hat{\sigma}_\alpha^l \tau \right) + \beta h_l \hat{\sigma}_\alpha^l + \beta \hat{\tau}_\alpha^l + \beta t_l \hat{\sigma}_\alpha^l \hat{\tau}_\alpha^l \right) \right\rangle_{\boldsymbol{\xi}^1} \cdots \right\rangle_{\boldsymbol{\xi}^k} \right\rangle_{\boldsymbol{\xi}}. \tag{31}$$

Performing the spin summations in the above equation and using the simple expression $F(\sigma_\alpha, \tau_\alpha) = \sum_{\sigma\tau} \delta_{\sigma,\sigma_\alpha} \delta_{\tau,\tau_\alpha} F(\sigma, \tau)$ to relocate the occurrences of σ_α and τ_α, we can take the limit $n \to 0$. The final result for the free energy (13) is then

$$f = -\frac{1}{\beta} \sum_{k=0}^{\infty} \frac{\mathrm{e}^{-c} c^k}{k!} \left\langle \left\langle \cdots \left\langle \int \left[\prod_{l=1}^{k} \mathrm{d}W_{\boldsymbol{\xi}^l}(h_l, r_l, t_l) \right] \right.\right.\right.$$
$$\left.\left.\left. \times \log \left[\sum_{\sigma\tau=\pm} \prod_{l=1}^{k} \frac{\Omega_{\sigma\tau}(h_l, r_l, t_l; \boldsymbol{\xi} \cdot \boldsymbol{\xi}^l)}{\mathcal{N}(h_l, r_l, t_l)} \right] \right\rangle_{\boldsymbol{\xi}^1} \cdots \right\rangle_{\boldsymbol{\xi}^k} \right\rangle_{\boldsymbol{\xi}} + \frac{c}{2\beta} \left\langle \int \mathrm{d}W_{\boldsymbol{\xi}}(h, r, t) \, \mathrm{d}W_{\boldsymbol{\xi}'}(h', r', t') \right.$$
$$\left. \times \log \left[\frac{\sum_{\tau\tau'=\pm} \cosh\left[\beta h + \beta t \tau + \frac{\beta}{c} (\boldsymbol{\xi} \cdot \boldsymbol{\xi}') \tau'\right] \cosh\left[\beta h' + \beta t' \tau' + \frac{\beta}{c} (\boldsymbol{\xi} \cdot \boldsymbol{\xi}') \tau\right] \mathrm{e}^{\beta r \tau + \beta r' \tau'}}{\sum_{\tau\tau'=\pm} \cosh[\beta h + \beta t \tau] \cosh[\beta h' + \beta t' \tau] \, \mathrm{e}^{\beta r \tau + \beta r' \tau'}} \right] \right\rangle_{\boldsymbol{\xi}\boldsymbol{\xi}'}. \tag{32}$$

5. Phase diagrams

5.1. Bifurcation analysis

The numerical observations concerning the densities $W_{\boldsymbol{\xi}}(h, r, t)$ in section 4 support the equivalence between the parallel and sequential versions of the finite-c Hopfield model. In

this section we will show further that one can analytically prove that the location of the second-order transitions between paramagnetic/spin-glass and paramagnetic/retrieval phases is identical to those of sequential dynamics.

Our bifurcation analysis is similar in spirit to [6]. First, we note that there exists a trivial solution $W_{\xi}(h,r,t)=\delta(h)\delta(r)\delta(t)$ that solves (29) for all $\boldsymbol{\xi}$, which is symmetric under the inversion of the fields $h\to -h, r\to -r$ and $t\to -t$. This solution, as can be easily confirmed, corresponds to the high-temperature paramagnetic state where no recall is possible and $m^{\sigma}_{\xi}=m^{\tau}_{\xi}=0$. As the temperature is lowered from $T=\infty$ we expect non-trivial solutions to bifurcate from the paramagnetic one. The new solutions can either preserve the previous inversion symmetry (spin-glass solution) or not (ferromagnetic solution). To determine the transition temperature at which these new solutions occur we first assume that close to the transition $\int \mathrm{d}W_{\xi}(h,r,t)h^{\ell}=\mathcal{O}(\epsilon^{\ell})$, $\int \mathrm{d}W_{\xi}(h,r,t)r^{\ell}=\mathcal{O}(\epsilon^{\ell})$ and $\int \mathrm{d}W_{\xi}(h,r,t)t^{\ell}=\mathcal{O}(\epsilon^{\ell})$. We can then expand equation (24) and identify term by term each expression in the resulting power series on the left- and right-hand sides of (24). To second order, this one-to-one correspondence first indicates that integrals carrying the field t must vanish. We then obtain

$$\int \mathrm{d}W_{\xi}(h,r,t)h = c\left\langle \int \mathrm{d}W_{\xi'}(h,r,t)h\tanh\left[\frac{\beta}{c}(\boldsymbol{\xi}\cdot\boldsymbol{\xi}')\right]\right\rangle_{\xi'} \tag{33}$$

$$\int \mathrm{d}W_{\xi}(h,r,t)r = c\left\langle \int \mathrm{d}W_{\xi'}(h,r,t)r\tanh\left[\frac{\beta}{c}(\boldsymbol{\xi}\cdot\boldsymbol{\xi}')\right]\right\rangle_{\xi'} \tag{34}$$

$$\int \mathrm{d}W_{\xi}(h,r,t)h^2-\left[\int \mathrm{d}W_{\xi}(h,r,t)h\right]^2 = c\left\langle \int \mathrm{d}W_{\xi'}(h,r,t)h^2\tanh\left[\frac{\beta}{c}(\boldsymbol{\xi}\cdot\boldsymbol{\xi}')\right]\right\rangle_{\xi'} \tag{35}$$

$$\int \mathrm{d}W_{\xi}(h,r,t)r^2-\left[\int \mathrm{d}W_{\xi}(h,r,t)r\right]^2 = c\left\langle \int \mathrm{d}W_{\xi'}(h,r,t)r^2\tanh\left[\frac{\beta}{c}(\boldsymbol{\xi}\cdot\boldsymbol{\xi}')\right]\right\rangle_{\xi'}. \tag{36}$$

These four equations mark the different types of transitions away from the paramagnetic state. The first pair of equations will give us the transition from $m^{\sigma}_{\xi}=0$ and $m^{\tau}_{\xi}=0$ respectively to a non-trivial recall (ferromagnetic) state whereas the second pair will give us the transition to the spin-glass state[5]. The resulting similarity in the first and second pair of the above equations is a consequence of the equivalence of the two species of spins in our system.

Now, to determine the critical parameter values for which these transitions occur we need to evaluate the highest temperature for which the following $2^p\times 2^p$ matrices have an eigenvalue equal to 1:

$$M_{\xi\xi'}=cp_{\xi'}\tanh\left[\frac{\beta}{c}(\boldsymbol{\xi}\cdot\boldsymbol{\xi}')\right] \qquad Q_{\xi\xi'}=cp_{\xi'}\tanh^2\left[\frac{\beta}{c}(\boldsymbol{\xi}\cdot\boldsymbol{\xi}')\right]. \tag{37}$$

These equations are identical to those found in [6]. An elegant construction of the eigenvalues of matrices of the above form (which relies on exploiting the properties $M_{\xi\xi'}=M(\boldsymbol{\xi}\cdot\boldsymbol{\xi}')$ and $Q_{\xi\xi'}=Q(\boldsymbol{\xi}\cdot\boldsymbol{\xi}')$) has already been given in [17]. Here, we state the final result determining the transition lines, identical to that found in [6]:

$$\mathrm{P}\to\mathrm{R}: \quad \frac{c}{2^p p}\sum_{m=0}^{p}\binom{p}{m}(p-2m)\tanh\left[\frac{\beta}{c}(p-2m)\right]=1 \tag{38}$$

[5] Note that the integrals over the cross terms between the fields, as for instance $\int \mathrm{d}W_{\xi}(h,r,t)ht$ are not relevant, neither in the paramagnetic/retrieval nor in the paramagnetic/spin-glass transition. In the first case they are $\mathcal{O}(\epsilon^2)$, whereas in the latter the symmetry of the density $W(h,r,t)$ under the inversion of the fields ensures that the corresponding integrals vanish identically.

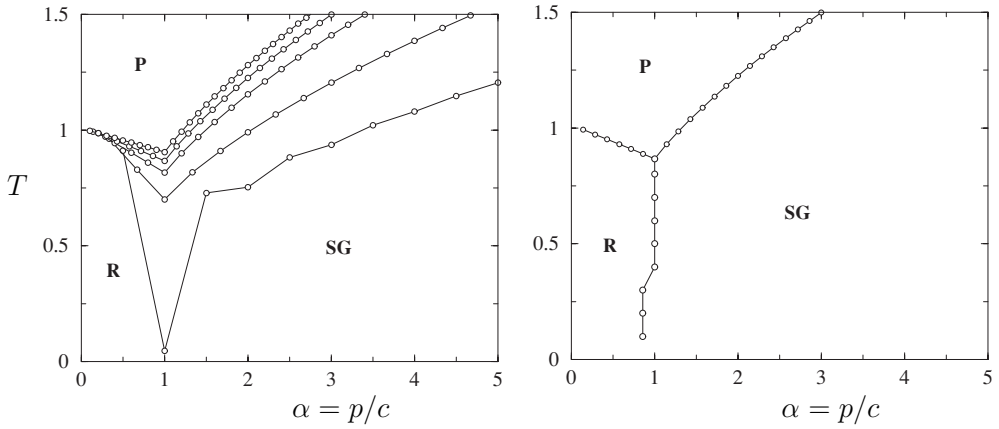

Figure 2. Phase diagram of the finite-connectivity Hopfield model with synchronous dynamics in the (α, T) plane. Left: the paramagnetic/retrieval and paramagnetic/spin-glass transition lines as obtained from the bifurcation analysis. (from lower to upper lines $c = \{2, 3, 5, 7, 10\}$). Right: the $c = 7$ phase diagram with the spin-glass/retrieval transition line (obtained by direct evaluation of the pattern overlaps (19) using population dynamics). Markers correspond to integer p values (lines are simply put as guides to the eye). On the retrieval/spin-glass transition line $m_\sigma = m_\tau = 0$.

$$\mathrm{P} \to \mathrm{SG}: \quad \frac{c}{2^p} \sum_{m=0}^{p} \binom{p}{m} \tanh^2 \left[\frac{\beta}{c}(p - 2m) \right] = 1. \tag{39}$$

In general, the bifurcation analysis cannot be applied to determine the spin-glass/retrieval transition line which must be computed directly from equations (29) and (19). This numerical task becomes increasingly difficult for large values of the connectivity parameter c (since one is required to evaluate 2^p sublattice densities where $p \simeq c$ close to the spin-glass/retrieval transition). For sufficiently small values of the connectivity parameter c (up to $c = 7$) we find that this transition line is identical to that of sequential dynamics. It is interesting to note that within replica-symmetric considerations, the $c \to \infty$ (extremely-diluted) phase diagrams of sequential and parallel Hopfield models are not identical, indicating that a critical $c_\star$ exists above which $W_\xi^t(t)$ is no longer given by $\delta(t)$. Determining this transition is a challenging numerical task.

5.2. Results and comparison with simulations

By numerically solving equations (19) and (29) we find that only one magnetization component (also called pattern overlap) m_λ^μ (16) provides non-trivial solutions (i.e. only one pattern is retrieved while the others are zero). For notational simplicity, we will from now on denote these non-zero solutions simply as m_σ and m_τ.

Plotting solutions of (38) and (39) in the (α, T) plane (with $\alpha = p/c$) results in the phase diagram of figure 2. It has been plotted for $c \in \{2, 3, 5, 7, 10\}$ and it consists of three phases: a high-temperature paramagnetic phase with all observables identically zero, a retrieval phase with $m_\sigma, m_\tau \neq 0$ and $q_{\lambda\lambda'} = 0$ (with $\lambda = \sigma, \tau$) and a spin-glass phase with $m_\sigma = m_\tau = 0$ and $q_{\lambda\lambda'} \neq 0$.[6] For $T \leqslant 1$ the spin-glass/retrieval transition is obtained numerically by direct evaluation of our observables.

We see that already for $c = 10$ (upper line) the phase diagram resembles closely the one derived in the extremely-diluted model [1] where the transition lines are given by $T = 1$ for

[6] Note that due to the inequality $q_{\alpha_1\alpha_2} \geqslant q_{\alpha_1\alpha_2\alpha_3\alpha_4} \geqslant \cdots \geqslant 0$ we only need to examine $q_{\alpha_1\alpha_2}$ to identify the spin-glass phase.

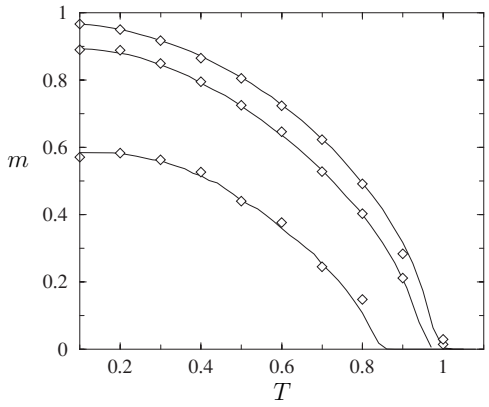

Figure 3. Pattern overlaps $m_\sigma = m_\tau = m$ as functions of $T = 1/\beta$ calculated from equations (19) and (29). Parameter values are: $p = 2$ and $c = \{3, 5, 7\}$ (from lower to upper lines). Markers correspond to simulation experiments of $N = 10\,000$ neurons.

$\alpha \leqslant 1$ (P $\to$ R) and $T = \sqrt{\alpha}$ for $\alpha \geqslant 1$ (P $\to$ SG). From the perspective of neural network operation, this shows that sparsely connected models retain the same qualitative features for a wide variety of synaptic connections per neuron and can retrieve information even for surprisingly small values of connections.

In figure 3 we present solutions of the sublattice overlap m_σ (19) and m_τ showing the second-order transition from retrieval to paramagnetic states for the simplest non-trivial case of $p = 2$. These have been drawn for $c = \{3, 5, 7\}$ showing the effect of different degrees of connectivity on the retrieval success. To verify our results we have performed simulation experiments on the dynamical process (1) for a system size of $N = 10\,000$ neurons (markers of figure 3). These appear to be in very good agreement with our theory. The simulation experiments also show that while Hebbian-type couplings (4) lead to fixed-point stationary solutions, anti-Hebbian ones where $J_{ij} = -\frac{c_{ij}}{c}(\boldsymbol{\xi}_i \cdot \boldsymbol{\xi}_j)$ lead to 2-cycles with $m_\sigma(t) = -m_\sigma(t+1)$ (and similarly for m_τ). Also, evaluation of the free energy (32) as a function of temperature T shows that it is a monotonically decreasing function indicating that the entropy remains positive even for low temperatures.

We have also compared our pattern overlaps with those derived from the analysis of [6] (which has as a starting the Ising 'sequential' Hamiltonian) and within the accuracy of numerical precision we have found that observables of the two systems are identical. This result, although somewhat expected given both knowledge from earlier neural network studies and, of course, the identity of our bifuraction results with those of [6], is also a bit surprising: in the process of solving our equations we introduced a 3D RS 'effective-field' distribution (compared to the 1D sequential one of [6]). As it turns out however the system in the process of updating fields by iteration of (29) effectively discards those which describe species correlations and factorizes $W_{\boldsymbol{\xi}}(h, r, t)$ to $W_{\boldsymbol{\xi}}(h, r)\delta(t)$. Henceforth, our 3D RS field distribution reduces to a 2D one. The equivalent treatment of $\boldsymbol{\sigma}$ and $\boldsymbol{\tau}$ then ensures (as also in analytically simpler models) that equilibrium observables between sequential and synchronous systems are identical (this relation, however, ceases to exist for a certain large value $c_\star$ since for $c \to \infty$ the sequential and parallel phase diagrams *are* different [8]).

In figure 4 we have plotted the pattern overlaps m_σ^μ and m_τ^μ as a function of α for different values of the temperature (note that $m_\sigma^\mu = m_\tau^\mu$) . We have set the average connectivity to $c = 7$ while varying the number of patterns p (therefore the number of pattern overlaps m^μ also

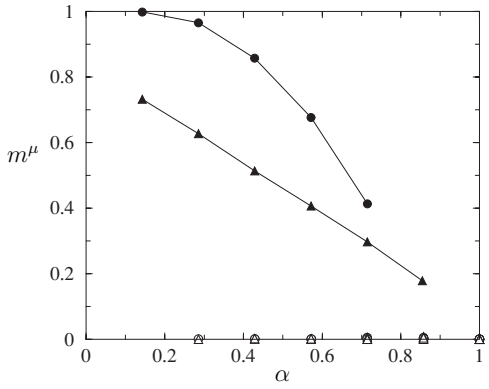

Figure 4. Pattern overlap $m^\mu_\sigma = m^\mu_\tau = m^\mu$ as a function of α (with $c = 7$) for $T = 0.1$ (circles) and $T = 0.7$ (triangles). Here we can see the first-order transition from retrieval to the spin-glass phase at $\alpha = 6/7$ and $\alpha = 7/7$ for $T = 0.1$ and $T = 0.7$ respectively.

changes with α). From this graph we can complete the phase diagram (figure 2), determining the location of the first-order transition from retrieval to spin-glass states.

6. Discussion

In this paper we have studied equilibrium properties of attractor neural network models with finite connectivity in which neurons operate in a parallel way. This work is motivated by the interesting properties that the two types of dynamical models share in simpler (e.g. fully-connected) scenarios: there, and for a surprisingly large number of universality classes, one can prove analytically that the equilibrium states following from the two different dynamical rules are identical. Our starting point here is the Peretto Hamiltonian (3). We have followed on the footsteps of [6] to derive the transition lines in our phase diagram and expressions for the (sublattice) overlaps. The resulting phase diagram plotted in the (α, T) plane then consists of three phases: a high-temperature paramagnetic phase, a retrieval and a spin-glass phase. The transitions from the paramagnetic phase have been determined analytically while the first-order retrieval/spin-glass transition has been computed using population dynamics [18]. Under our replica-symmetric considerations we have shown that the retrieval properties of the parallel finite-connectivity Hopfield model are identical to those of the sequential one. Comparison with numerical simulations for large system sizes shows excellent agreement.

Many questions remain to be answered for neural networks of finite connectivity. Using the same framework (as initiated by [6]) one can proceed further with the study of multi-state e.g. Q-Ising or Blume–Emery–Griffiths neural networks. A different approach would be to study systems which consist of two species of operating units (as, effectively, here) but which explicitly interact with one another. This would lead us to an Ashkin–Teller-type neural network in which the phase diagram can be different. Non-trivial extensions would be to study the validity of the RS solution following the schemes in [21, 22]. These will be the subject of a future work.

Acknowledgments

We are indebted to Bastian Wemmenhove and Toni Verbeiren for very helpful discussions and the Fund for Scientific Research-Flanders, Belgium. IPC thanks the Abdus Salam ICTP for

hospitality and NSS wishes to thank Professor D Bollé for supporting this research. We would like to thank one of the referees for useful remarks.

References

[1] Canning A and Naef J P 1992 *J. Physique* I **2** 1791
[2] Viana L and Bray A J 1985 *J. Phys. C: Solid State Phys.* **18** 3037
[3] Kanter I and Sompolinsky H 1987 *Phys. Rev. Lett.* **58** 164
[4] Monasson R and Zecchina R 1998 *Phys. Rev.* E **56** 1357
[5] Kabashima Y and Saad D 1999 *Europhys. Lett.* **45** 97
[6] Wemmenhove B and Coolen A C C 2003 *J. Phys. A: Math. Gen.* **36** 9617
[7] Müller B and Reinhardt J (ed) 1990 *Neural Networks, An Introduction (Physics of Neural Networks Series)* (Berlin: Springer)
[8] Verbeiren T *PhD Thesis* (in preparation)
[9] Fontanari J F and Köberle R 1988 *J. Physique* **49** 13
[10] Watkin T L H and Sherrington D 1991 *Europhys. Lett.* **14** 791
[11] Watkin T L H and Sherrington D 1991 *J. Phys. A: Math. Gen.* **24** 5427
[12] Nishimori H TITECH report (unpublished)
[13] Bollé D, Carlucci D M and Shim G M 2000 *J. Phys A: Math. Gen.* **33** 6481
[14] Theumann WK and Erichsen R 2001 *Phys. Rev.* E **64** 061902
[15] Derrida B, Gardner E and Zippelius A 1987 *Europhys. Lett.* **4** 167
[16] Peretto P 1984 *Biol. Cybern.* **50** 51
[17] van Hemmen J L and Kühn R 1986 *Phys. Rev. Lett.* **57** 913
[18] Mezard M and Parisi G 2001 *Eur. Phys. J.* B **20** 217
[19] Vicente R, Saad D and Kabashima Y 1999 *Phys. Rev.* E **60** 5352
[20] Coolen A C C 2001 *Handbook of Biological Physics* vol 4 ed F Moss and S Gielen (Amsterdam: Elsevier) pp 531–96
[21] Monasson R 1998 *J. Phys. A: Math. Gen.* **31** 513
[22] Montanari A and Ricci-Tersenghi F 2003 *Eur. Phys. J.* B **33** 339